CONFERENCE PRE-PRINT

INTEGRATED NUMERICAL ANALYSIS OF IMPURITY TRANSPORT AND SOURCES FOR HIGH CURRENT-HIGH POWER BASELINE PULSES WITH T IN JET-ILW

I. IVANOVA-STANIK

Institute of Plasma Physics and Laser Microfusion

Warsaw, Poland

Email: irena.ivanova-stanik@ifpilm.pl

A. CHOMICZEWSKA

Institute of Plasma Physics and Laser Microfusion

Warsaw, Poland

E. KOWALSKA-STRZECIWILK

Institute of Plasma Physics and Laser Microfusion

Warsaw, Poland

L. GARZOTTI

CCFE, Culham Science Centre

Abingdon, United Kingdom

G. PUCELLA

Dip.to Fusione e Tecnologie per la Sicurezza Nucleare, ENEA C. R. Frascat

Frascati (Roma), Italy

G. TELESCA

Institute of Plasma Physics and Laser Microfusion

Warsaw, Poland

D. VAN EESTER

LPP-ERM/KMS, Association EUROFUSION-Belgian State, TEC partner

Brussels, Belgium

R. ZAGÓRSKI

National Centre for Nuclear Research

Otwock, Poland

V.K.ZOTTA

Department of Astronautical, Electrical and Energy Engineering, Sapienza University of Rome

Rome, Italy

JET CONTRIBUTORS¹

and THE EUROFUSION TOKAMAK EXPLOATATION TEAM²

¹ see the author list of 'Overview of T and D-T results in JET with ITER-like wall" by C.F. Maggi et al. 2023 Nucl. Fusion 63 110201

² See the author list of "Overview of the EUROfusion Tokamak Exploitation programme in support of ITER and DEMO" by E. Joffrin et al. 2024 Nucl. Fusion 64 112019

Abstract

The work describes integrated numerical modelling applied to JET-ILW high current – high power baseline pulses with tritium with tungsten divertor and beryllium wall in corner configuration using the COREDIV code, which self-consistently solves 1D radial transport equations of plasma and impurities in the core region and 2D multi-fluid transport in the scrape-off layer. Simulation indicated that for considered experimental pulses, the increase of the radiation in the core plasma is due to the change of the impurity transport in core plasma and not due to the increase of the impurity source. The simulations show that sputtering of W due to T is negligible. For beryllium ions, the dominant contribution to W sputtering is due to Be^{2+} .

1. INTRODUCTION

Presently planned fusion reactors (DEMO [1], STEP [2], SPARC [3]) intend to work with a mixed fuel of deuterium (D) and tritium (T). In the last decades almost all devices operated with hydrogen and deuterium. JET has been an exception due to its ability to operate with tritium [4]. Experiments with a deuterium and tritium fuel mix are crucial for the ITER. Only two magnetic confinement fusion devices have ever had the capability to handle tritium; JET and TFTR. [6].

At the end of 2021 the JET-ILW (ILW=ITER-like wall, with a tungsten divertor and a beryllium main chamber) tokamak revisited to deuterium-tritium operations during the so-called "DTE2 campaign" [7]). In DTE2 two main scenarios were exploited with the goal of achieving fusion power higher than 10 MW for 5 s: the baseline scenario relying on high plasma current ($I_p = 3.5$ MA) and stronger magnetic field ($B_T = 3.35$ T), to achieve good confinement [8], the hybrid scenario with lower current ($I_p \le 3.0$ MA) [9]. The baseline plasmas are characterized by relatively low normalized beta ($\beta_N < 2$) and edge safety factor q_{95} ($q_{95} \approx 3$) compared to the alternative optimized hybrid scenario ($\beta_N > 2$, $q_{95} \approx 4.8$.).

The development of the baseline scenario in tritium (T) was motivated by the need to investigate the effects of the isotope mixture on the underlying physics of the scenario, to explore isotope-dependent effects: power threshold, impurity contents etc. We remind that, the baseline scenario has been successfully developed for high performance in D for 5 s, but it has not been possible to sustain this same scenario could for more than 1–2 s in T and 3 s in D–T [8, 10].

In JET-ILW discharges many impurities are usually observed: high Z (tungsten (W), molybdenum (Mo)) originating in the divertor region, middle Z-impurities (nickel (Ni), copper (Cu)) and low Z (beryllium (Be)) from the wall, nitrogen (N), neon (Ne) and argon (Ar) from puffing and helium (He) from fusion reactions [11]. All scenarios are occasionally affected by heavy impurity accumulation, the most dangerous of which is the tungsten (W). The development of scenarios must address a the related challenge: the control of the accumulation of the radiating tungsten in the plasma core. One possible way to reduce tungsten (W) impurity influx is by lowering the target temperature through strike-point sweeping. The strike point location on the outer target is swept radially by $\Delta R \sim 3$ cm at 4 Hz for baseline scenario while ICRH also has to be used in high-power H-mode JET-ILW discharges, both to avoid core impurity accumulation [12].

The investigation of impurity behaviour and understanding of the causes that led to an uncontrolled increase of radiated power, were one of the crucial issues and prepared as discussed in Ref.[13], when study the impact of total heating power, flat-top gas flow and ELM (edge localized modes) frequency on Ni, Cu and W. The tungsten (W) content in the plasma is governed by a balance between the influx of W impurities from the scrape-off layer (SOL), driven by inward neoclassical convection across the pedestal, and their removal or "flushing" from the plasma by edge-localized modes (ELMs). This behavior for the deuterium (D) baseline scenario is reported in Ref. [14]. The highest confinement Baseline D pulse and the D–T pulse ($I_p = 3.5$ MA and $P_{in} \approx 35$ MW) were analysed in Ref. [15] and numerically simulated with the aim of determining whether the differences in their behaviour could be explained by differences in impurity transport and sources.

In this paper we concentrate on the analysis of the baseline scenario in T plasma for shots #99268 and #99282. For this aim COREDIV code is used, which self-consistently simulates the core and scrape off layer (SOL) plasma. Mutual interactions of both regions are of great importance for the case with W divertor when the energy balance depends strongly on the coupling between bulk and the SOL. The analysis focuses on investigating the mechanisms responsible for the increase in radiated power during these pulses, with particular emphasis on impurity transport and tungsten (W) production. The study examines the W concentration in the plasma, the impact of impurity transport in the core plasma on W production, the level of W sputtering induced by beryllium (Be) and nickel (Ni), and the profile of the effective charge (Z_{eff}).

2. THE COREDIV MODEL

Simulations were performed using the COREDIV code (a full description of the code can be found in Ref. [16]), which is based on an integrated approach coupling radial transport in the core with 2D multifluid dynamics in the scrape-off layer (SOL). As this work is a continuation of our previous studies [15, 17], only the key aspects of the model are summarized here.

The anomalous diffusion coefficients for impurities and main ions are assumed to be equal. The convection velocity for impurities—taken to be the same for all impurity species and ionization states—is treated as an input parameter and adjusted to reproduce the experimentally measured radiation profiles. The radiation density profile can be numerically reconstructed by applying an outward (positive) convection velocity in the plasma core and an inward (negative) convection at the plasma edge.

The simulations consider four impurity species: beryllium (Be), neon (Ne), nickel (Ni), and tungsten (W). The input parameters for the code include the fluxes of Be, Ne, and Ni. In contrast, the W flux is calculated self-consistently, depending on the fluxes and energies of Be, Ne, and Ni, and includes self-sputtering and prompt redeposition.

Continuity of energy and particle fluxes as well as of particle densities and temperatures at the separatrix are imposed for the coupling between the core and SOL modules This condition is particularly important for tungsten, which is generated mainly via sputtering by both main ions and impurities (in all ionization states) in the SOL, but radiates predominantly in the core plasma.

The weak point of the COREDIV code is that is assumes slab geometry and that the same transport coefficient are adopted for all impurities and all ionization states.

3. EXPERIMENT AND SIMULATIONS

This study presents a numerical analysis of baseline discharges with a total auxiliary heating of approximately 30 MW, conducted in the ITER-like wall (ILW) corner configuration, without impurity seeding. The analyzed discharges #99268 and #99282 were performed in Tritium (T) plasmas at the same plasma current of 3.5 MA and a toroidal magnetic field of 3.25 T.

The impact of the higher isotope mass on the baseline scenario could only be tested either with gas puff only or by using H pellets. The 2 mm Hydrogen pellets have been launched from a flight line located at the upper high-field side of the main vessel. The primary distinction between the pulses lies in the hydrogen pellet injection rate, which is 25 Hz for pulse #99268 and varies between 35 Hz and 17 Hz during pulse #99282 and significant different in beam power as well.

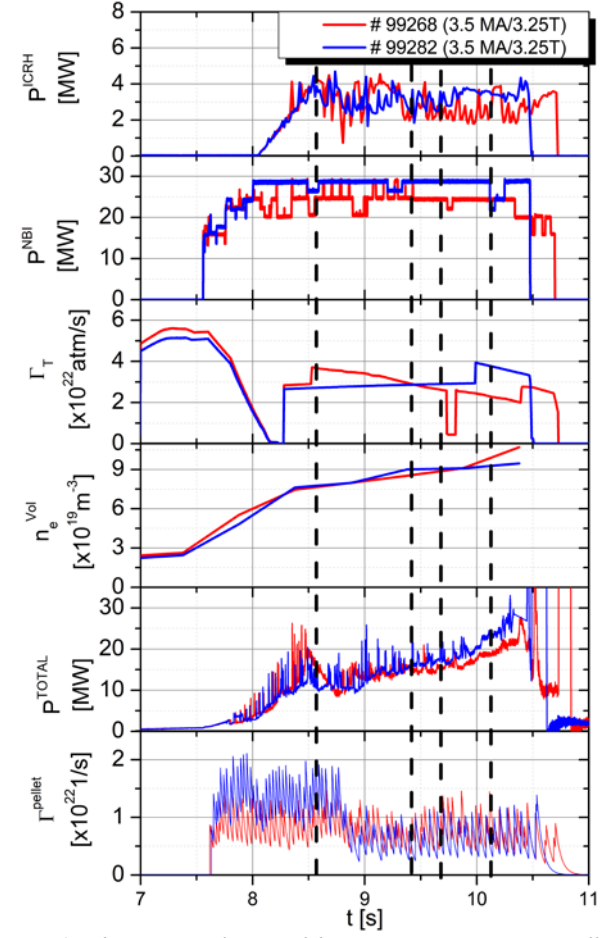


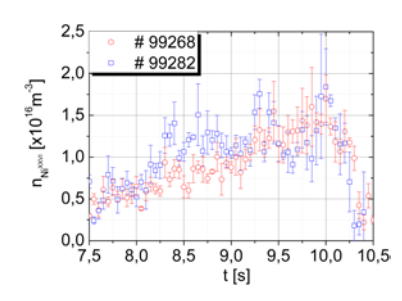
Fig.1. The time evolution of heating power, Tritium puff, electron volume-averaged density (n_e^{VOL}), total radiated power (P^{TOTAL}), and pellet flux for pulses #99268 and #99282.

Fig. 1 shows the time evolution of auxiliary power (ICRH (P^{ICRH}) +NBI (P^{NBI}) heating), T puff level (Γ_T), electron volume-average density (n_e^{VOL}) from LIDER, total radiated power, and pellet flux (Γ^{pellet}) for both pulses #99268 and #99282, highlighting the intervals during which hydrogen pellets were injected. This data provides an overview of the heating conditions and the pellet injection patterns that are critical for understanding the observed plasma behavior. While the ICRH power is the same in the two pulses, for the # 99282 pulse the NBI power is about 4 MW lower than the #99268. The dashed vertical lines indicate the times (t = 8.6 s, 9.4 s, 9.7 s and 10.08

s) at which the numerical simulations are performed for the two pulses. For both pulses observed increase on the electron density and of the radiated power after the 8.7 s, which, after having exceeded the level of the heating power, leads to the discharge disruption. For both pulses radiation fraction (f^{RAD}) increase from 50% at time t=8.6s to 65-70% at t = 10.08 s.

Spectroscopy diagnostics collected by the VUV survey spectrometer [18] are used for identification of impurities (more in particular for Nickel (Ni)) and the determination on its density and concentration in the plasma. The experimental Ni density (n_{Ni}) for two normalize radii r/a = [0.5, 0.6] based on the Ni^{XXVI} and r/a = [0.85, 0.95] based on the Ni^{XXVII} is presented in Fig. 2 and Fig. 3, respectively. Due to the high neutron rate in D–T plasmas, the vacuum ultraviolet (VUV) spectrometer and the soft X-ray (SXR) cameras, used for measuring the tungsten density along the plasma radius were disconnected. Moreover, using data from the above-mentioned spectrometer to extract meaningful information from the VUV spectra [19] – in particular monitoring the wavelengths 140-260 Å associated with W-ions W¹⁴⁺ – W³⁵⁺ - the approach was employed to calculate W intensity I_W . The time evolution of the W intensity for analyzed pulses is shown in Fig. 3. Note that W¹⁴⁺ – W³⁵⁺ in the corona distribution is in the temperature range 0.1 keV -2.6 keV, which for this shots is for normalized radius r/a = [0.6, 1.0] (see Fig.5).

In the experiments, an increase in Ni density (n_{Ni}) by a factor of about 2 is observed in both shots from t = 8.6 s to t = 10.0 s. However, the W intensity shows only small changes between 8.6 s and 9.8 s is small changes, but then increases by a factor of two between 9.8 s and 10.08 s. The increase in W intensity is associated with higher radiation in mantle region (see Fig.5.) from the low field side (LFS) of the plasma.



99268 # 99282 0 7,5 8,0 8,5 9,0 9,5 10,0 10,5

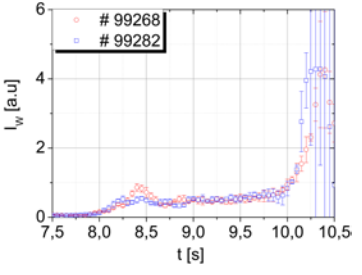


Fig.2. The experimental Ni density for pulses #99268 and #99282 based on the Ni^{XXVI} spectral line.

Fig.3. The experimental Ni density for pulses #99268 and #99282 based on the Ni^{XVII} spectral line.

Fig.4. The W intensity for pulses #99268 and #99282

The numerical results of this study are compared with experimental data, primarily based on measurements from the bolometry diagnostic [20]. At times t = 8.6 s, 9.4 s, 9.7 s, and 10.08 s, Fig. 5 presents bolometric tomographic reconstructions of the radiated power density for pulse #99268. Tritium pulses are often characterized by a time dependent increase in the radiated power in the mantle region (0.70 < r/a < 0.95). These reconstructions highlight an increase in radiated power in the plasma core, reflecting changes in the overall plasma behavior as the discharge evolved. No increase in radiation is observed in the central region of the plasma.

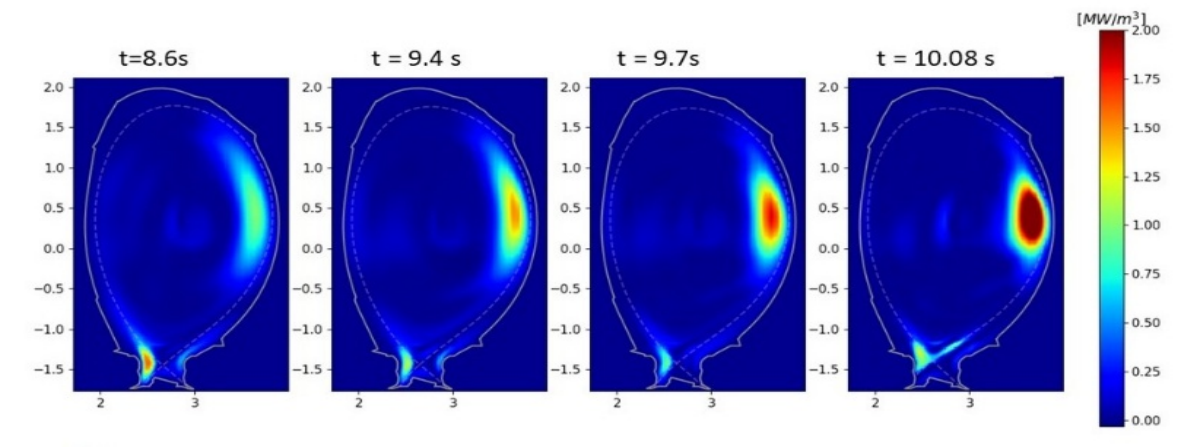


Fig. 4. Tomographic reconstructions of the radiated power density at times t = 8.6 s, 9.4 s, 9.7 s, and 10.08 s for pulse #99268.

Sawtooth (ST) oscillations alter the behavior of central plasma temperature and density profiles and influence impurity transport, due to the correlation between changes in MHD activity and impurity transport [21]. The sawtooth dynamics in JET baseline discharges with Deuterium (D), Tritium (T), and D-T mixtures was investigated to assess confinement during high-beta operations at 3.5 MW, 3.3 T, and $q_{95} = 3$ The sawtooth instabilities period tends to increase with high isotope mass [22].

The MHD analysis for pulse #99268 is shown in Fig. 5. This pulse is characterized by core n = 1 activity (sawtooth, fishbones and inter-ST 1/1 mode) as well as by the presence of an outboard radiative blob leading to edge cooling and finally a 2/1 locked mode. The n=3 component in the spectrogram (green track) is the third harmonic of the inter-sawtooth 1/1 mode as well as the n=2 component in the spectrogram (blue track) is the second harmonic. The only ST-triggered modes in the pulse are a short-lived n=4 and an n=5, both triggered by the sawtooth at 10.27 s. During the analyzed period, sawtooth crashes observed at t=8.65 s and t=9.475 s have no impact on confinement. It should be noted that the analyzing time frame falls outside the main ST period.

COREDIV simulations were performed using an integrated approach that couples radial impurity transport in the core plasma with a 2D multifluid model of the scrape-off layer (SOL). The simulations included four impurities: Be, W, Ni and Neon (Ne). In JET-ILW, Ne is routinely used in charge exchange recombination spectroscopy (CXRS) for ion temperature measurements.

In the simulation, the choice on the Ni and Ne puff level is to reproduce experimental Ni and Ne concentration. The simulation setup assumed impurity transport coefficients, with 'ad-hoc' convective velocities for impurity used to match the experimental radiated power profiles and the radiation in bulk and SOL plasma.

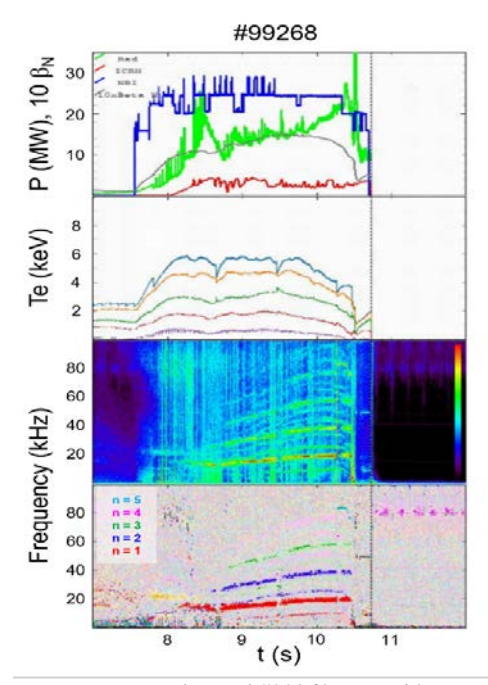


Fig. 5.MHD analysis of #99268: NBI (blue) and ICRH (red) powers, total radiated power (green) and normalised beta (grey), electron temperature at different radii, spectrogram of mode amplitudes and (d) spectrogram of toroidal mode numbers from Mirnov coils.

To compare the results of our simulations with the experimental data we have to rely essentially on the high-resolution Thomson scattering (HRTS) diagnostic [23], for measurement of the electron density (n_e) and temperature profiles (T_e), and on the charge exchange recombination spectroscopy (CXRS) for the measurement of the ion temperature (T_i) profile. The experimental and simulated profiles of the electron and ion density and temperatures are shown in Fig.6. for four times at which analysis was performed. In the experiment, a gradual increase in the electron density is observed from analyzing time t = 8.6 s to t=10.08s, along with increase in the diamagnetic energy (W_{dia}) from 6.8 MJ at t = 8.6s to 8.6 MJ at t = 9.4s, as estimated by EFIT [24]. This increase in energy corresponded to a rise in temperatures (ion and electron) between r/a = 0 and r/a = 0.4 (see Fig. 6). After t = 9.4s decreasing again, reaching 6.8MJ at t 10.08s. This decrease is consistent with the reduction observed in both electron and ion temperatures.

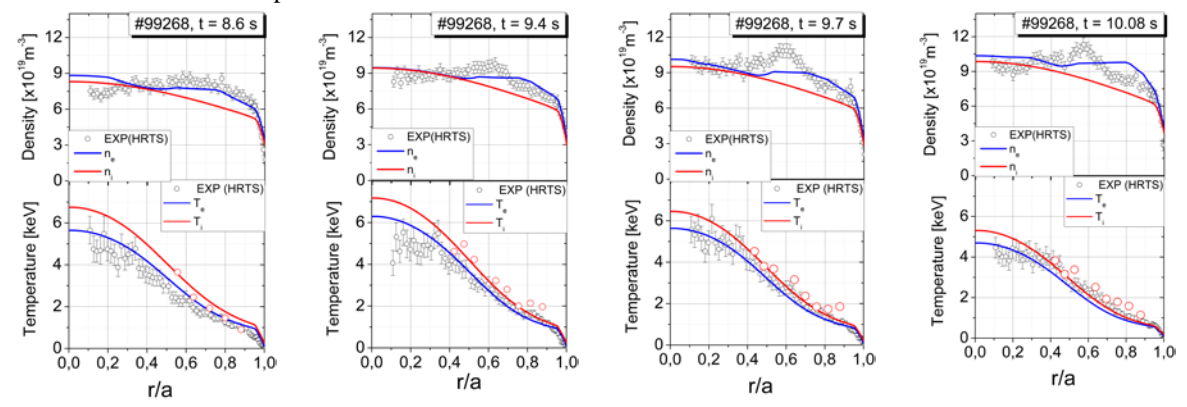


Fig.6. Experimental data and the corresponding COREDIV modelling results: electron density (n_e) profile and electron (T_e) as well as ion (T_i) temperature profiles for the pulse #99268 at four times.

Although neon is expected to be quickly removed during experiments in which it is used, it becomes embedded in plasma-facing components and is continuously released afterwards. In the analyzed discharges, no neon puffing was applied, yet neon is still experimentally detected. The Ne and Ni puff level remains unchanged throughout the first three analyzed time points. For the last point, when a lower temperature is observed on the divertor plate (lower power to divertor) the input flux for Ne, Ni and Be is reduced by 50%. The Ne experimental concentration of fully ionized Ne (C_{Ne}^{10+}) is shown in Fig.7. The C_{Ne}^{10+} values are initially low but increase over time. At r/a = 0.6, the concentration rises from 0.03% at t = 8.6 s to 0.075% at t = 10.08 s. According to simulations, the contribution of neon radiation in the core is very small compared to the total radiated power: 0.04 MW vs. 11.5 MW at t = 8.6 s, and 0.23 MW vs. 15.8 MW at t = 10.08 s. Neon sputtering is calculated at 1.2×10^{18} atom/s contributing only 6.2% to the total sputtering yield (including main ions and all impurities) at t = 8.6 s. This decrease to 1.1×10^{18} atom/s, which is 10 % of the total sputtering yield at t = 10.08 s. It is also noted that the electron temperature at the strike point decreases from 21.7 eV at t = 8.6 s to 14.7 eV at t = 10.08 s. The W sputtering by T is 0.07% at t = 8.6 s and go to 0 % for t = 10.08 s, but from Be is 71% no changes for analysing time. For beryllium ions, the dominant contribution to W sputtering is due to Be²⁺.

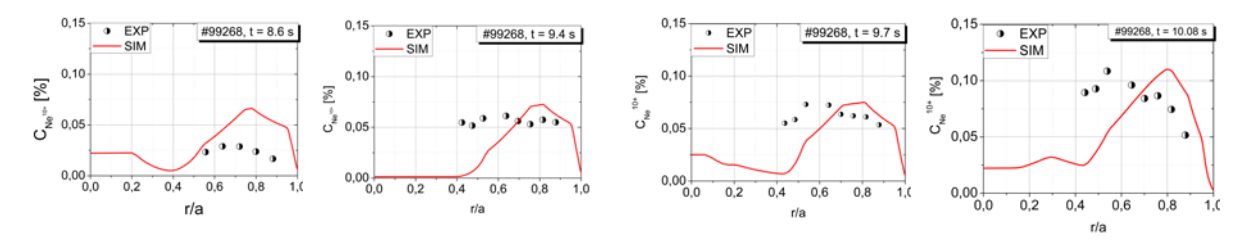


Fig. 7. The experimental and simulated Ne concentration for four time t = 8.6s, 9.4s, 9.7s and 10.08s for pulse #99268.

Fig. 8. Shows the experimental and simulated profiles of radiation power, impurity pinch-to-diffusion coefficient ratio, impurity densities for W, Ne, Be and Ni (both simulated and experimental, based on the Ni^{XXVI}) and the effective charge (Z_{eff}) profiles from simulation at analyzed time t = 8.6 s, 9.4s, 9.7s and 10.08s for pulse #99268. The numerical results presented in Fig. 8 indicate an increase in the density of Ni over time, despite the constant flux input of Ni. In contrast, the W density remains relatively stable throughout the pulse, primarily due to the self-consistently calculated reduction in the W flux by the COREDIV model.

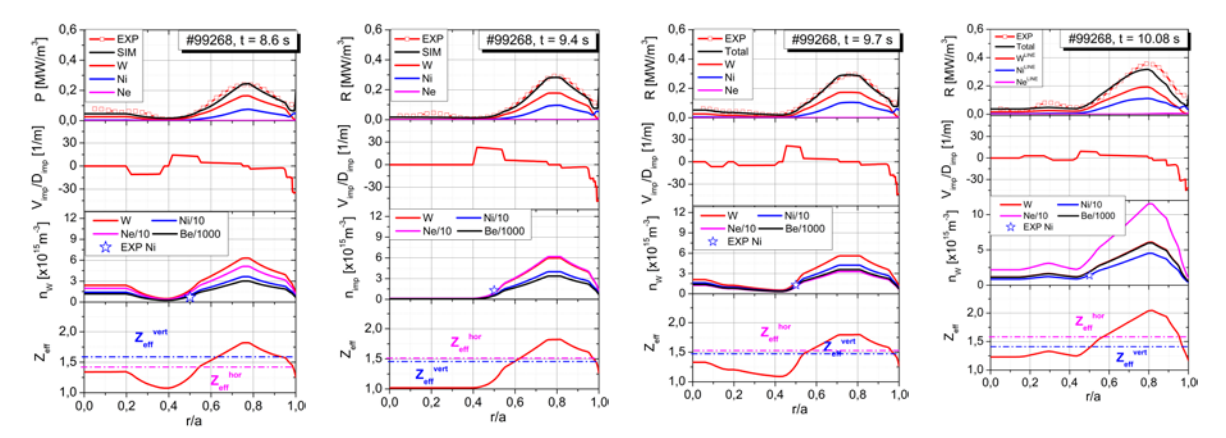


Fig.8. Experimental and simulated radiation power profile, impurity pinch-to-diffusion coefficient ratio, impurity densities: simulated (line) and experimental density based on the Ni^{XXVI} (star) and affective charge ($Z_{\rm eff}$) profiles from simulation at analyzed times t=8.6 s, 9.4s, 9.7s and 10.08s for pulse #99268.

The profiles for Ni and W radiation reveal distinct behaviors, with the maximum W radiation located at $r/a \approx 0.6$ –0.9, resulting from inward convective velocities in the edge region and outward velocities in the core region. Significant changes in impurity inward pinch are observed around t = 10.08 s, likely related to the loss of edge localized modes (ELMs), which are attributed to excessive radiated power. In summary, the results from the COREDIV simulations provide valuable insights into impurity transport processes and the role of tungsten in the radiative power increase observed during the discharges.

There are three factors that influence of the changes in radiation: changes in the impurity density (n_{imp}) by source or transport, second: electron density and third: cooling factor (Q), which depend by electron temperature. A first suggestion is that the radiation increases in time because increase the electron density (see Fig 6), but increasing is about 10%. Second factor, while the Ni density increases over time, the W intensity remains constant (see

I.IVANOVA-STANIK et al.

Fig.2), primarily due to the effects of impurity transport and the self-consistent modeling of impurity flux dynamics within COREDIV. To reproduce the core radiation profile we have two pinches: outward pinch from $r/a\sim0.4$ to $r/a\sim0.55$ (see Fig.8) and inward pinch r/a=[0.95-1.0], which effects the impurity profiles. The W concentration decreases by about a factor 1.5 between t=8.6 s to t=10.8s, dropping from 5.2×10^{-5} to 3.86×10^{-5} , respectively. In contrast, the total W radiation increase is small from 7.5 MW to 8.9 MW, about 15%. The Ni radiation increase from 3.0 MW to 5.7 MW. The Z_{eff} profile has a maximum for r/a=[0.6-0.9]. The simulations show that sputtering of W due to T is negligible. For beryllium ions, the dominant contribution to W sputtering is due to Be²⁺

According to the simulations, for the experimental pulses studied, the observed increase in core plasma radiation results primarily from modifications in impurity transport between the pedestal and the separatrix, rather than from an enhanced impurity source. The W content in the core plasma depends on several factors: the source in the divertor plate, transport in the SOL plasma and core plasma, and the ELM frequency. ELM crashes can transport W out of the pedestal region, and the ELM frequency is a key parameter which can be used to avoid W influx to the bulk plasma [25]. However, it has also been shown that ELMs contribute to W sputtering, and are a significant part of the source [26].

The results of this study are consistent with the findings in [27, 28], where radiation control strategies also focused on managing impurities to avoid excessive radiated power. However, the current study provides a more detailed analysis of W transport. Comparing the results for T plasma with those for D and DT plasma reported in Ref. [2] for the Baseline scenario, it can be concluded that the behaviour of DT plasma is similar to that of T plasma. In both cases, the radiation density profile can be numerically reconstructed by assigning a positive pinch velocity in the central plasma (outwards) and a negative convection at the plasma edge (inwards). In T plasma similar to DT outward pinch decrease in the time, but with increase inward pinch increase. This increase is possibility to connected to the change in ELM frequence. Both exhibits relatively stable W concentrations, despite differences in impurity transport mechanisms, indicating that the main factors influencing the radiative power are similar across these plasma types. This is associated with the different ELM dynamics, which exhibit a lower frequency, smaller amplitude, and more complex structure compared to Deuterium and Deuterium-Tritium plasmas [27, 28].

CONCLUSION

The COREDIV code has been used to simulate JET-ILW high current – high power baseline discharges with different core transport models, with a particular focus on the influence of impurity inward pinch on the radiation levels and tungsten production in the SOL. Good agreement was found between experimental data and COREDIV results in terms of densities, temperatures, and radiation profiles.

Simulations indicated that, for the experimental pulses considered, the increase in core plasma radiation is primarily due to changes in impurity transport between the pedestal and the separatrix, rather than an increase in the impurity source. This behavior is associated with different ELM dynamics, which exhibit lower frequency, smaller amplitude, and a more complex structure compared to Deuterium and Deuterium-Tritium plasmas.

Tritium operation suffers from higher radiation levels and, consequently, higher impurity content compared to D and D-T plasmas [13]. Simulations showed that this increased radiation is not connected to enhanced sputtering due to the higher isotope mass — since, for divertor plate temperatures of 10–22 eV, sputtering by Tritium is negligible. The increased radiation may instead be attributed to the development of hollow density profiles (observed in both DT and T plasmas), which can affect plasma transport — leading to an outward particle pinch in the core and reduced ELM frequency, thereby decreasing impurity flushing and enhancing the inward impurity pinch. Therefore, for ITER, controlling the ELM frequency will be crucial to maintaining H-mode, especially in high-density scenarios

ACKNOWLEDGEMENTS

This scientific paper has been published as part of the international project co-financed by the Polish Ministry of Science and Higher Education within the programme called 'PMW'.

This work has been carried out within the framework of the EUROfusion Consortium, funded by the European Union via the Euratom Research and Training Programme (Grant Agreement No 101052200 — EUROfusion). Views and opinions expressed are however those of the author(s) only and do not necessarily reflect those of the European Union or the European Commission. Neither the European Union nor the European Commission can be held responsible for them.

REFERENCES

- [1] FEDERICI G. et al., Overview of the design approach and prioritization of R&D activities towards an EU DEMO, Fusion Engineering and Design 109–111 (2016) 1464–1474
- [2] CHAPMAN I et al. Overview of the STEP Programme in the UK. Fusion Engineering and Design, 146 (2019): 1642–1645.
- [3] GREENWALD M. et al. The SPARC tokamak: Conceptual design. Journal of Plasma Physics, 86 (2020): 865860502.
- [4] RIMINI F et al 2025 40 years of JET operations: a unique contribution to fusion science Plasma Phys. Control. Fusion 67 033001
- [5] DONNÉ A.J.H. et al. European research roadmap to the realization of fusion energy, https://euro-fusion.org/wp-content/uploads/2022/10/2018_Research_roadmap_long_version_01.pdf.
- [6] STRACHAN J D et al 1997 TFTR DT experiments Plasma Phys. Control. Fusion 39 B103
- [7] MAGGI C (JET Contributors) 2024 Overview of T and D-T results in JET with ITER-like wall Nucl. Fusion 64 112012
- [8] GARZOTTI L. et al., Development of high-current baseline scenario for high deuterium-tritium fusion performance at JET, Plasma Phys. Control. Fusion **67** (2025) 075011
- [9] HOBIRK J. et al., Hybrid scenario for JET DTE2, accepted for publication in Nuclear Fusion special issue on JET T and D-T experiments Nucl. Fusion 63 (2023) 112001
- [10] GARZOTTI Let al., Development of high-current baseline scenario for deuterium- tritium high fusion performance at JET, 29th IAEA Fusion Energy Conference, 16-21 October 2023, London, United Kingdom.
- [11] KRAWCZYK N. et al., Application of the VUV and the soft x-ray systems on JET for the study of intrinsic impurity behaviour in neon seeded hybrid discharges Rev. Sci. Instrum. (2018) 89, 10D131
- [12] LERCHR E et al., Optimization of ICRH for core impurity control in JET-ILW 2016 Nucl. Fusion 56 036022
- [13] WENDLER N. et al., Impurity behaviour in JET high-current baseline scenario for Deuterium, Tritium and Deuterium-Tritium plasmas, Nuclear Materials and Energy 41 (2024) 101743
- [14] FIELD A R et al., The impact of fuelling and W radiation on the performance of high-power, ITER-baseline scenario plasmas in JET-ILWPlasma Phys. Control. Fusion 63 (2021) 095013
- [15] TELESCa G. et al., COREDIV simulations of D and D–T high current–high power Baseline pulses in JET-ITER like wall Nucl. Fusion **64** (2024) 066018
- [16] ZAGORSKI R., IVANOVA-STANIK R.I. and STANKIEWICZ R. Simulations with the COREDIV code of DEMO discharges2013 Nucl. Fusion 53 073030
- [17] IVANOVA-STANIK I.et al., Influence of the impurities in the hybrid discharges with high power in JET ILW, Nucl. Fusion 62 (2022) 066010 (9pp).
- [18] COFFEY I.H. et al., First tritium operation of ITER-prototype VUV spectroscopy on JET Rev. Sci. Instrum. 75 (2004)3737.
- [19] LAWSON KD et al., Impurity analysis of JET DiMPle pulses, Plasma Phys. Control. Fusion 63 (2021) 105001
- [20] HUBER A, et al., Upgraded bolometer system on JET for improved radiation measurements, Fusion Eng. Design 82 (2007) 1327–1334
- [21] PORCELLI F et al 1996 Model for the sawtooth period and amplitude, Plasma Phys. Control. Fusion 38 2163
- [22] NOWAK S. et al 2023 Sawteeth dynamics in JET Baseline discharges with mixtures of isotopes 2023 29th IAEA Fusion Energy Conf. (London, United Kingdom, 16–21 October 2023)
- [23] PASQUALOTTO R et al., High resolution Thomson scattering for joint European torus (JET) . 2004 *Rev. Sci. Instrum.* **75** 3891–3
- [24] SZEPESI G. et al 2021 Advanced equilibrium reconstruction for JET with EFIT++ 47th EPS Conf. Plasma Physics (Stiges, Spain (virtual conference), 21–25 June 2021) P 3.1037 (available at: http://ocs.ciemat.es/EPS2021PAP/pdf/P3.1037.pdf)
- [25] DUX R., Janzer A. and Pütterich T., Main chamber sources and edge transport of tungsten in H-mode plasmas at ASDEX Upgrade 2011 Nucl. Fusion 51 053002
- [26] DEN HARDER N et al., ELM-resolved divertor erosion in the JET ITER-Like Wall 2016 Nucl. Fusion 56 026
- [27] PIRON L. et al., Radiation control in deuterium, tritium and deuterium-tritium JET baseline plasmas part I Fusion Engineering and Design 193 (2023) 113634
- [28] PIRON L. et al., Radiation control in deuterium, tritium and deuterium-tritium JET baseline plasmas part II Fusion Fusion Engineering and Design 192 (2023) 113695